Onset and Progression in Inherited ALS Determined by Motor Neurons and Microglia

Séverine Boillée,[1]* Koji Yamanaka,[1]*† Christian S. Lobsiger,[1] Neal G. Copeland,[2] Nancy A. Jenkins,[2] George Kassiotis,[3]‡ George Kollias,[3] Don W. Cleveland[1]†

Dominant mutations in superoxide dismutase cause amyotrophic lateral sclerosis (ALS), a progressive paralytic disease characterized by loss of motor neurons. With the use of mice carrying a deletable mutant gene, expression within motor neurons was shown to be a primary determinant of disease onset and of an early phase of disease progression. Diminishing the mutant levels in microglia had little effect on the early disease phase but sharply slowed later disease progression. Onset and progression thus represent distinct disease phases defined by mutant action within different cell types to generate non–cell-autonomous killing of motor neurons; these findings validate therapies, including cell replacement, targeted to the non-neuronal cells.

Amyotrophic lateral sclerosis (ALS) is an adult-onset neurodegenerative disease that selectively kills upper and lower motor neurons. Dominant mutations in the gene encoding the ubiquitously expressed superoxide dismutase (SOD1) are the most prominent known causes of inherited ALS (*1*). Several hypotheses to explain motor neuron degeneration have been proposed, including mitochondrial dysfunction, protein aggregate formation, excitotoxicity, axonal transport malfunction, mutant-derived oxidative damage, lack of growth factors, and inflammation (*2*). Ubiquitous expression of mutant SOD1 in rodents leads to a progressive selective degeneration of motor neurons because of an acquired toxic property or properties (*3*–*5*). However, the contribution of damage mediated by mutant SOD1 to disease onset and progression in specific cell types of the spinal cord is not established. Expression of mutated SOD1 selectively in either motor neurons (*6*, *7*) or astrocytes (*8*) has failed to cause ALS-like disease in mice. Although reducing SOD1 mutant accumulation within motor neurons by viral-delivered small interfering RNA can slow disease onset (*9*, *10*), disease progression was not affected except in one case in which it was accelerated (*10*). Indeed, analyses of chimeric mice composed of mixtures of normal and SOD1 mutant–expressing cells have offered evidence that motor neuron death is non–cell-autonomous, with normal non–motor-neuronal cells having the ability to reduce or eliminate toxicity to mutant-expressing motor neurons (*11*).

To identify which cell types are damaged by mutant SOD1 and how this damage might influence the initiation and propagation of the course of the disease, transgenic mice (LoxSOD1^{G37R}) were generated that carried a mutant human SOD1^{G37R} gene flanked at both ends by 34–base pair LoxP sequences allowing recognition and regulated deletion by the Cre recombinase (fig. S1A) (*12*). Mice developed fatal progressive motor neuron disease, including progressive weight loss from denervation-induced muscle atrophy and paralysis that was essentially indistinguishable from that seen in previously described SOD1^{G37R} lines (*5*). The LoxSOD1^{G37R} line with highest mutant accumulation reached end-stage disease most rapidly (between 8.5 and 11 months), which was accompanied by the death of 55% of spinal motor neurons (fig. S1, B to F) (*12*). No human SOD1 protein was expressed in any progeny from the LoxSOD1^{G37R} females that also carried a transgene encoding the Cre recombinase in their

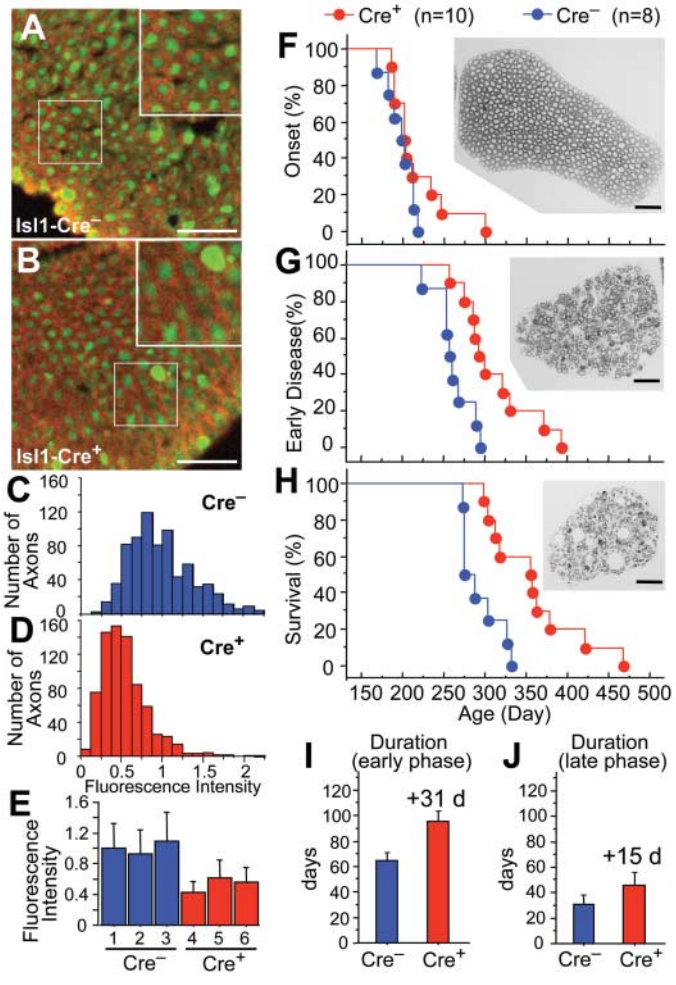

Fig. 1. Selective Cre-mediated gene inactivation shows that mutant SOD1 action within motor neurons is a primary determinant of an early disease phase. (**A** and **B**) Mutant SOD1 levels in motor axons of LoxSOD1^{G37R} mice in the (A) absence or (B) presence of Islet1-Cre expression. L5 ventral root sections were stained simultaneously with antibodies to (green) human SOD1 and (red) myelin basic protein. Insets show magnified images of boxed regions. (**C** and **D**) Histograms of relative intensities of mutant SOD1 fluorescence in each L5 motor axon measured from three (C) LoxSOD1^{G37R} or (D) LoxSOD1^{G37R}/Isl1Cre^{+} mice. (**E**) Total accumulated mutant SOD1 levels measured as relative total fluorescence intensity in motor axons from entire L5 roots in each animal (n = 3 for each genotype). (**F** to **H**) Ages of (F) disease onset, (G) progression through an early disease phase (to 10% weight loss), and (H) disease end stage of (red) LoxSOD1^{G37R}/Isl1Cre^{+} mice and (blue) LoxSOD1^{G37R} littermates. Insets show ventral root motor axons (stained with toluidine blue) in LoxSOD1^{G37R} mice at (F) onset, (G) early disease, and (H) end stage. (**I** and **J**) Duration of (I) an early disease phase (from onset to 10% weight loss) and (J) a later disease phase (from 10% weight loss to end stage) for (red) LoxSOD1^{G37R}/Isl1Cre^{+} and (blue) LoxSOD1^{G37R} littermates. Scale bars in (A), (B), and (F) to (H), 50 μm.

[1]Ludwig Institute for Cancer Research and Departments of Medicine and Neuroscience, University of California at San Diego, 9500 Gilman Drive, La Jolla, CA 92093, USA. [2]Mouse Cancer Genetics Program, National Cancer Institute–Frederick Cancer Research and Development Center, Frederick, MD 21702, USA. [3]Institute of Immunology, Biomedical Sciences Research Center Alexander Fleming, 166 72 Vari, Greece.

*These authors contributed equally to this work.
†To whom correspondence should be addressed. E-mail: dcleveland@ucsd.edu (D.W.C.); kyamanaka@ucsd.edu (K.Y.)
‡Present address: Division of Immunoregulation, National Institute for Medical Research, The Ridgeway, Mill Hill, London NW7 1AA, UK.

oocytes (*13*), demonstrating efficient in vivo gene removal in the presence of Cre (fig. S1, G and H) (*12*).

To examine the contribution to the disease of mutant SOD1 toxicity within motor neurons, LoxSOD1^{G37R} mice were mated to mice carrying a Cre-encoding sequence under control of the promoter from the Islet-1 transcription factor (*14*). Cre recombinase in this line is expressed in the nervous system exclusively in progenitors of motor and dorsal root ganglion neurons and was sufficient to substantially reduce mutant SOD1 accumulation in most motor axons of L5 motor roots and lumbar motor neurons of presymptomatic Isl1-Cre^{+}/LoxSOD1^{G37R} animals (Fig. 1, A to E, and fig. S2) (*12*).

A simple objective measure of the earliest onset of disease was defined by the peak of the weight curve (*12*, *15*). This age coincides with initial axonal retraction from neuromuscular synapses but occurs before substantial axonal degeneration or loss proximally in motor roots emerging from the spinal cord (Fig. 1F, inset). An early stage of disease, accompanied by hindlimb weakness and obvious axonal degeneration (Fig. 1G, inset), was defined to be the period from onset until denervation-induced muscle atrophy decreased maximal weight by 10%. Reduction of SOD1^{G37R} in motor neurons slowed disease onset in a minority of LoxSOD1^{G37R}/Isl1Cre^{+} mice, yielding an average delay of 18 days (Isl1Cre^{+}, 216 ± 11.2 days; Isl1Cre^{-}, 198 ± 6.1 days) (Fig. 1F). Progression from onset through early disease was delayed in all of the mice, with a mean extension of 31 days (Isl1Cre^{+}, 95 days; Isl1Cre^{-}, 64 days) (Fig. 1, G and I); there was also a more modest slowing of later disease progression, with a mean extension of 15 days (Fig. 1J). Overall survival was extended by 64 days (Isl1Cre^{+}, 357.5 ± 17.2 days; Isl1Cre^{-}, 293.5 ± 8.7 days) (Fig. 1H).

Microglia are the resident immune cells of the central nervous system and are the primary mediators of neuroinflammation (*16*). In the normal adult nervous system, these cells exist in a resting state and are characterized by a small cell body and fine ramified processes. However, neuronal damage can rapidly activate the release of cytotoxic and inflammatory mediators, including oxygen radicals, nitric oxide, and cytokines, that affect neighboring neurons and astrocytes (*16*, *17*); in ALS, strong activation and proliferation of microglia occur in regions of motor neuron loss (*18*, *19*). Minocycline, an antibiotic that can inhibit microglial activation (*20*), extends the survival of SOD1 mutant mice (*21*–*23*), as does the inhibition of cyclooxygenase 2 (COX-2) (*24*), a key enzyme in prostaglandin synthesis. Both findings have raised the possibility of direct microglial involvement in ALS.

To test the role of the SOD1 mutant acting within microglia, we generated mice expressing Cre selectively in these cells using the promoter for CD11b (*25*), an integrin expressed exclusively in the myeloid lineage (*26*) (fig. S3A) (*12*). Cell-type specificity of Cre expression was verified by mating those mice to the Rosa26 mouse line that ubiquitously expresses a β-galactosidase (β-Gal) transgene that can be translated into functional β-Gal only if Cre-mediated recombination removes a premature translation terminator (*27*). Peritoneal macrophages and microglial cells expressed β-Gal in Rosa26/CD11b-Cre^{+} mice, whereas no cells of either type expressed β-Gal in animals without the CD11b-Cre gene (fig. S3, B and D to G) (*12*). Although both neurons and astrocytes from Rosa26 mice showed high levels of β-Gal activity after germline Cre expression (Fig. 2B), only small microglia-like cells expressed β-Gal in mice with the CD11b-encoded Cre and no β-Gal expression was detectable in neurons or astrocytes (Fig. 2A).

CD11b-Cre expression significantly diminished SOD1^{G37R} accumulation in peritoneal macrophages of LoxSOD1^{G37R} animals (Fig. 2, C and D; n = 4 or 5 per group). Quantitative real-time fluorescence polymerase chain reaction (QPCR), capable of distinguishing as small as a 20% difference in human SOD1 transgene DNA number (fig. S3C) (*12*), confirmed that macrophages from CD11b-Cre^{+} animals retained only half of the mutant SOD1^{G37R} genes as did the Cre^{-} animals (Fig. 2C; n = 4 per group). Microglia, purified from 1-day-old LoxSOD1^{G37R}/CD11b-Cre^{+} mice or their Cre^{-}

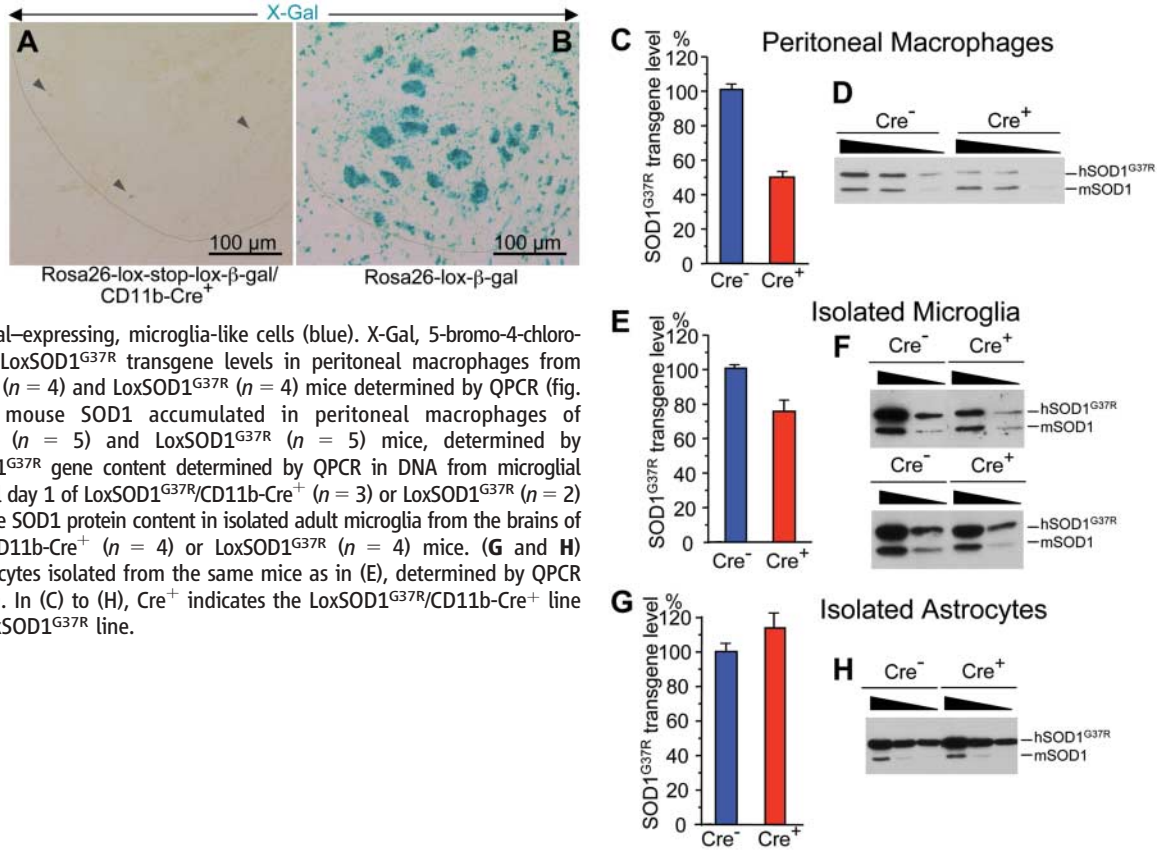

Fig. 2. CD11b-Cre–directed excision of SOD1^{G37R} exclusively in macrophage and microglial lineages. (**A** and **B**) β-Gal activity in lumbar spinal cord sections of (A) Rosa26/CD11b-Cre^{+} mice or (B) Rosa26 mice after systemic Cre-mediated gene excision. Arrowheads point to small, β-Gal–expressing, microglia-like cells (blue). X-Gal, 5-bromo-4-chloro-3-indolyl-D-galactoside. (**C**) LoxSOD1^{G37R} transgene levels in peritoneal macrophages from LoxSOD1^{G37R}/CD11b-Cre^{+} (n = 4) and LoxSOD1^{G37R} (n = 4) mice determined by QPCR (fig. S3C). (**D**) Human and mouse SOD1 accumulated in peritoneal macrophages of LoxSOD1^{G37R}/CD11b-Cre^{+} (n = 5) and LoxSOD1^{G37R} (n = 5) mice, determined by immunoblotting. (**E**) SOD1^{G37R} gene content determined by QPCR in DNA from microglial cells isolated from postnatal day 1 of LoxSOD1^{G37R}/CD11b-Cre^{+} (n = 3) or LoxSOD1^{G37R} (n = 2) mice. (**F**) Human and mouse SOD1 protein content in isolated adult microglia from the brains of 7-week-old LoxSOD1^{G37R}/CD11b-Cre^{+} (n = 4) or LoxSOD1^{G37R} (n = 4) mice. (**G** and **H**) SOD1^{G37R} content in astrocytes isolated from the same mice as in (E), determined by QPCR (G) or immunoblotting (H). In (C) to (H), Cre^{+} indicates the LoxSOD1^{G37R}/CD11b-Cre^{+} line and Cre^{-} indicates the LoxSOD1^{G37R} line.

littermates and then cultured for 2 weeks, showed a 25% Cre-dependent decrease in the SOD1^{G37R} transgene levels (Fig. 2E). A similar reduction in mutant SOD1 was seen in adult microglia (Fig. 2F). Mutant SOD1 transgene content was unchanged in purified astrocytes (Fig. 2, G and H).

Microglial activation begins at or before disease onset in mutant SOD1 mice (*21*, *28*, *29*), with the number of activated cells escalating during progression, as measured with antibodies to CD11b or Iba1 (Fig. 3, A to C). No differences in microglia (Fig. 3, D to F) or astrocyte (Fig. 3, G to I) activation were observed in disease-matched LoxSOD1^{G37R}/CD11b-Cre^{+} and LoxSOD1^{G37R} mice. Nevertheless, lowering mutant SOD1 expression within microglia significantly extended the survival of LoxSOD1^{G37R} mice, with a longer mean survival of 99 days relative to the cohort of LoxSOD1^{G37R} littermates (Fig. 3J). Half of the Cre-expressing cohort survived more than 100 days past the mean survival of LoxSOD1^{G37R} mice, and most of this extension was derived from slowing disease progression after onset. Indeed, although early disease progression was unchanged (Fig. 3K), the progression of later disease in CD11b-Cre^{+} mice was slowed by an average of 75 days (Fig. 3L). This slowing of later disease may derive in part from gene inactivation not just in microglia but also in peripheral macrophages or their progenitors and/or from the migration of those cells into the central nervous system after initial damage to motor neurons.

The potential for different mechanisms underlying disease initiation and progression has previously been proposed in human ALS from observations of disease spread from an initially affected region. Our use of partial, selective gene inactivation offers direct evidence for mutant SOD1 damage within different cell types to underlie an initiating phase of disease caused by mutant SOD1 damage within motor neurons, and a mechanistically divergent later phase encompassing the progression to complete paralysis that is linked to the inflammatory response of microglia and mutant toxicity within these cells. These findings have important implications for the development of successful therapies for mutant SOD1–mediated as well as sporadic ALS. Although the mechanistic linkage between familial and sporadic ALS has not been unambiguously established, the two forms of disease are clinically indistinguishable, affect the same neurons, are characterized by ubiquitinated aggregates as hallmarks, display a loss of astrocytic glutamate transporters, and are accompanied by microgliosis and astrocytosis (*2*). In our study, limiting mutant damage to microglia robustly slowed the disease's course, even when all motor neurons were expressing high levels of a SOD1 mutant. Thus, although the initiation of the disease requires damage to motor neurons and probably to additional cell types, disease therapy might be successful by targeting only a single non-neuronal cell type.

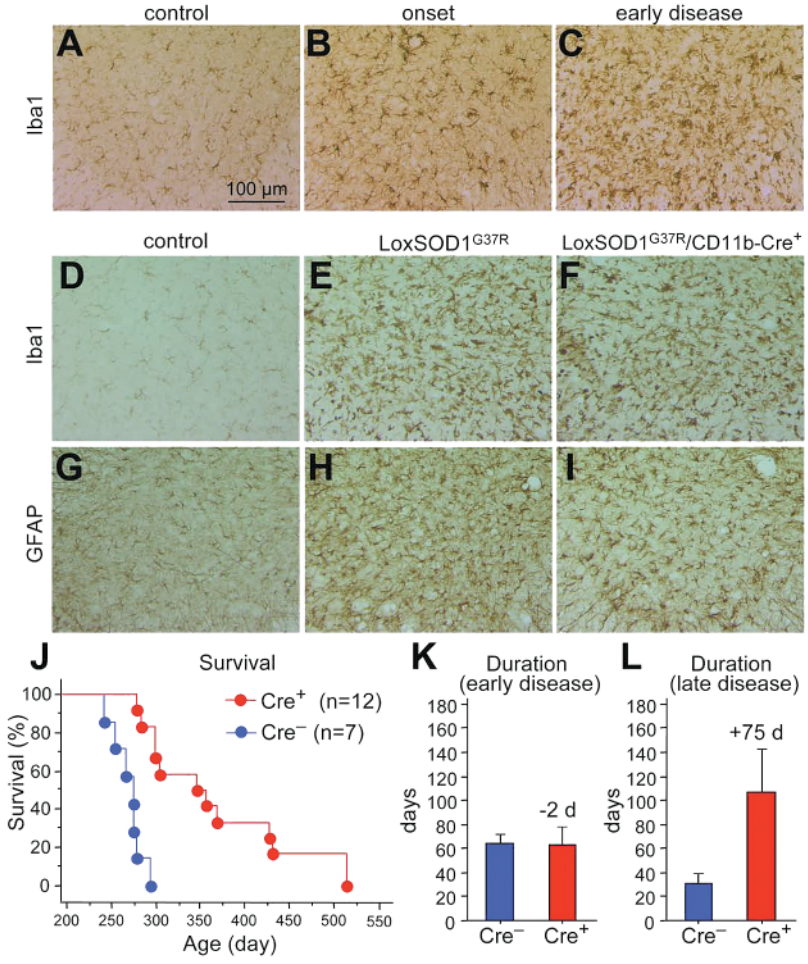

Fig. 3. Selective gene excision shows that mutant SOD1 action within the microglial and macrophage lineages is a primary determinant of a late phase of disease progression. (**A** to **C**) Microglial activation in the lumbar spinal cord of a LoxSOD1^{G37R} mouse at (B) disease onset and (C) an early disease stage (defined as 10% weight loss) compared to (A) that in an age-matched normal littermate. (**D** to **F**) Microglial activation in the lumbar spinal cord of (D) a normal mouse and of disease-matched (E) LoxSOD1^{G37R} or (F) LoxSOD1^{G37R}/CD11b-Cre^{+} mice, detected with antibodies to Iba1. (**G** to **I**) Astrocytes in the lumbar spinal cord of the same mice as in (D) to (F), detected with antibodies to glial fibrillary acidic protein (GFAP). (**J**) Survival times of LoxSOD1^{G37R}/CD11b-Cre^{+} (Cre^{+}) and littermate LoxSOD1^{G37R} (Cre^{-}) mice. (**K** and **L**) Disease duration of LoxSOD1^{G37R}/CD11b-Cre^{+} mice compared to LoxSOD1^{G37R} mice for (K) an early phase or (L) a late phase of disease.

References and Notes

1. D. R. Rosen *et al.*, *Nature* **362**, 59 (1993).
2. L. I. Bruijn, T. M. Miller, D. W. Cleveland, *Annu. Rev. Neurosci.* **27**, 723 (2004).
3. L. I. Bruijn *et al.*, *Neuron* **18**, 327 (1997).
4. M. E. Gurney *et al.*, *Science* **264**, 1772 (1994).
5. P. C. Wong *et al.*, *Neuron* **14**, 1105 (1995).
6. M. M. Lino, C. Schneider, P. Caroni, *J. Neurosci.* **22**, 4825 (2002).
7. A. Pramatarova, J. Laganiere, J. Roussel, K. Brisebois, G. A. Rouleau, *J. Neurosci.* **21**, 3369 (2001).
8. Y. H. Gong, A. S. Parsadanian, A. Andreeva, W. D. Snider, J. L. Elliott, *J. Neurosci.* **20**, 660 (2000).
9. T. M. Miller *et al.*, *Ann. Neurol.* **57**, 773 (2005).
10. G. S. Ralph *et al.*, *Nat. Med.* **11**, 429 (2005).
11. A. M. Clement *et al.*, *Science* **302**, 113 (2003).
12. See supporting material on *Science* Online.
13. M. Lewandoski, K. M. Wassarman, G. R. Martin, *Curr. Biol.* **7**, 148 (1997).
14. S. Srinivas *et al.*, *BMC Dev. Biol.* **1** (2001); available at www.biomedcentral.com/1471-213X/1/4.
15. J. Liu, L. A. Shinobu, C. M. Ward, D. Young, D. W. Cleveland, *J. Neurochem.* **93**, 875 (2005).
16. G. W. Kreutzberg, *Trends Neurosci.* **19**, 312 (1996).
17. U. K. Hanisch, *Glia* **40**, 140 (2002).
18. J. S. Henkel *et al.*, *Ann. Neurol.* **55**, 221 (2004).
19. T. Kawamata, H. Akiyama, T. Yamada, P. L. McGeer, *Am. J. Pathol.* **140**, 691 (1992).
20. J. Yrjanheikki *et al.*, *Proc. Natl. Acad. Sci. U.S.A.* **96**, 13496 (1999).
21. J. Kriz, M. D. Nguyen, J. P. Julien, *Neurobiol. Dis.* **10**, 268 (2002).
22. L. Van Den Bosch, P. Tilkin, G. Lemmens, W. Robberecht, *Neuroreport* **13**, 1067 (2002).
23. S. Zhu *et al.*, *Nature* **417**, 74 (2002).
24. D. B. Drachman *et al.*, *Ann. Neurol.* **52**, 771 (2002).
25. D. D. Hickstein, D. M. Baker, K. A. Gollahon, A. L. Back, *Proc. Natl. Acad. Sci. U.S.A.* **89**, 2105 (1992).
26. A. Mazzone, G. Ricevuti, *Haematologica* **80**, 161 (1995).

27. P. Soriano, *Nat. Genet.* **21**, 70 (1999).
28. M. E. Alexianu, M. Kozovska, S. H. Appel, *Neurology* **57**, 1282 (2001).
29. E. D. Hall, J. A. Oostveen, M. E. Gurney, *Glia* **23**, 249 (1998).
30. We gratefully acknowledge D.S. Howland (Molecular Genetics, Wyeth Research, Princeton, NJ 08543–8000) for the QPCR protocol; M. Mallat (U495, IFR70, INSERM UPMC, Paris, France) and V. Zujovic (UMR 546, INSERM UPMC, Paris, France) for advice on microglial cell culture; D. Swing for pronuclear injection; J. Folmer for tissue sections; and T. Jessel, G. Martin, and P. Soriano for Islet1-Cre, ZP3-Cre, and Rosa26 reporter mice, respectively. This work was supported by grants from NIH (NS 27036), the Center for ALS Research at Johns Hopkins, the ALS Association, and the European Commission (LSHG-CT-2005-005203). S.B. is a recipient of a Fondation pour la Recherche Medicale fellowship and an INSERM fellowship. K.Y. is a recipient of a Uehara Memorial Foundation fellowship and a Development grant from the Muscular Dystrophy Association.

Supporting Online Material
www.sciencemag.org/cgi/content/full/312/5778/1389/DC1
Materials and Methods
SOM Text
Figs. S1 to S3
References

6 December 2005; accepted 27 April 2006
10.1126/science.1123511

An SNP Caused Loss of Seed Shattering During Rice Domestication

Saeko Konishi,[1]* Takeshi Izawa,[2]* Shao Yang Lin,[1]† Kaworu Ebana,[2] Yoshimichi Fukuta,[3] Takuji Sasaki,[2] Masahiro Yano[2]‡

Loss of seed shattering was a key event in the domestication of major cereals. We revealed that the *qSH1* gene, a major quantitative trait locus of seed shattering in rice, encodes a BEL1-type homeobox gene and demonstrated that a single-nucleotide polymorphism (SNP) in the 5′ regulatory region of the *qSH1* gene caused loss of seed shattering owing to the absence of abscission layer formation. Haplotype analysis and association analysis in various rice collections revealed that the SNP was highly associated with shattering among *japonica* subspecies of rice, implying that it was a target of artificial selection during rice domestication.

Cultivation of major cereals likely started about 10,000 years ago (*1*–*4*). During this domestication, ancient humans subjected several key events to selection. These included increase in the number of seeds, improvement of fertility, change in plant architecture, change in seed shape, adaptation of flowering time to local areas, loss of seed color, and loss of seed shattering.

Recent studies in rice have revealed that several independent domestication events might have occurred to establish cultivated rice (*3*, *5*–*7*). The archaeological record reveals that *japonica* rice, a subspecies of *Oryza sativa*, was bred about 10,000 years ago in the upstream regions of the Yangtze River in southwest China (*3*, *8*, *9*).

The loss of seed-shattering habit is thought to be one of the most important events in rice domestication, because the "easy-to-shatter" trait in wild relatives results in severe reduction in yield. Over the course of human history, distinct grain-threshing systems have been developed in several different eras in local areas of the world, in accordance with the degree of seed shattering. In current rice-breeding programs, this seed-shattering habit is still a target, especially in the construction of new *indica* (another subspecies of *O. sativa*) cultivars. Thus, seed-shattering habit is one of

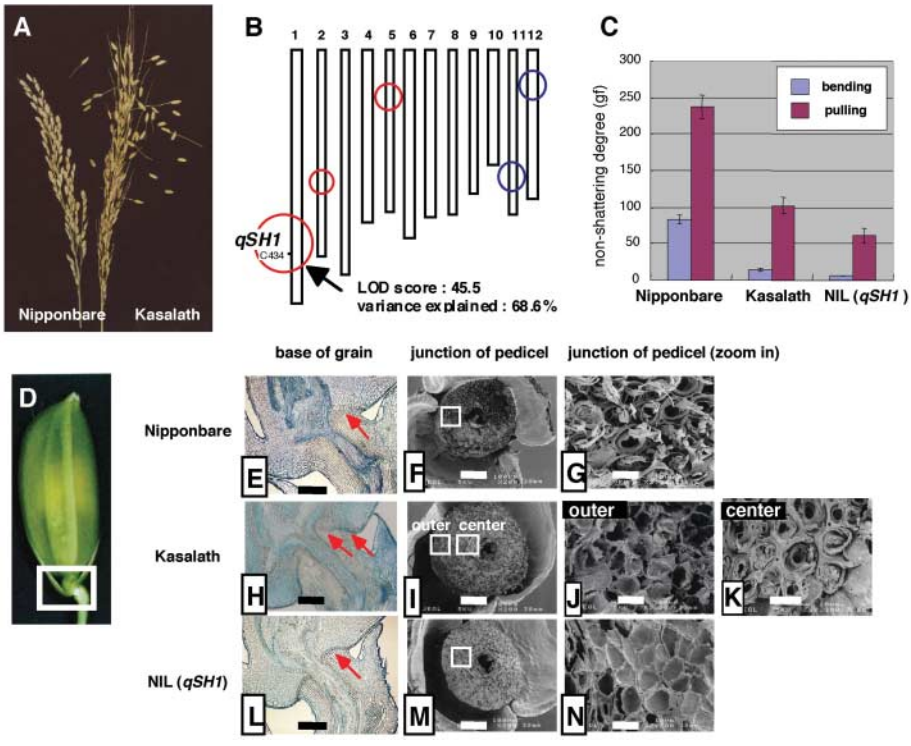

Fig. 1. *qSH1* is required for formation of the abscission layer at the base of the rice grain. (**A**) Seed-shattering habits of rice panicles. Photos taken after grabbing rice panicles. (Left) Nonshattering-type cultivar, Nipponbare. (Right) Shattering-type cultivar, Kasalath, in which the seed has shattered. (**B**) Chromosomal locations of QTLs for seed-shattering degree, based on an F_2 population from a cross between Nipponbare and Kasalath. Positions of circles indicate positions of QTLs, and circle size indicates the relative contribution of each QTL. Red circles, Nipponbare alleles contributing to non-shattering habit; blue circles, Kasalath alleles contributing to nonshattering. *qSH1* is marked on chromosome 1 with the nearest DNA marker (C434). (**C**) Non–seed-shattering habits of Nipponbare, Kasalath, and NIL(*qSH1*). Breaking tensile strength upon detachment of seeds from the pedicels by bending and pulling was measured (*10*). Increase in value indicates loss of shattering. NIL(*qSH1*), a nearly isogenic line carrying a Kasalath fragment at the *qSH1* locus in the Nipponbare background, as shown in fig. S1A. (**D**) Photo of a rice grain. White box indicates position of abscission layer formation. (**E** to **G**) Nipponbare. (**H** to **K**) Kasalath. (**L** to **N**) NIL(*qSH1*). (E), (H), and (L) Longitudinal sections of positions corresponding to white box in (D). Arrows point to the partial abscission layer of Kasalath in (H), the complete abscission layer of NIL(*qSH1*) in (L), and the corresponding region of Nipponbare in (E). (F), (I), and (M) Scanning electron microscope (SEM) photos of pedicel junctions after detachment of seeds. (G), (J), (K), and (N) Close-up SEM photos corresponding to white boxes in (F), (I), and (M). (G) Broken and rough surface of Nipponbare when forcedly detached. (N) Peeled-off and smooth surface of NIL(*qSH1*) upon spontaneous detachment. In Kasalath, rough center surface (K) and smooth outer surface (J) are observed. Scale bars: 500 μm in (E), (H), and (L); 100 μm in (F), (I), and (M); 10 μm in (G), (J), (K), and (N).